HIGH-SPEED TEST RIG FOR THE INVESTIGATION OF EROSION DAMAGE OF AXIAL COMPRESSOR BLADES

M. Schrade, S. Staudacher
Institute of Aircraft Propulsion Systems, University of Stuttgart, Germany

Abstract

Performance and maintenance characteristics of aircraft engines are highly influenced by erosion caused by ingested, solid particles. Axial compressor blades are vulnerable to erosion in particular since they are exposed to high relative fluid velocities and high particle concentrations. To be able to understand erosion phenomena in axial compressors, experimental work is indispensable. This paper presents a high-speed erosion test rig, which meets compressor specific boundary conditions in materials, fluid velocity and temperature. We present the design process and the commissioning of the test rig. Furthermore, erosion results with flat plates out of Ti6AlV4, which is a standard material for blades of the first stages of common axial high-pressure compressors, are discussed. The plates are eroded with a standardized test dust at fluid velocities of $300\,\mathrm{m\,s^{-1}}$ and $350\,\mathrm{m\,s^{-1}}$. The erosion of Ti6AlV4 showed typical patterns for ductile metals. We concluded that the high-speed test rig is able to fundamentally and reproducibly investigate erosion damage under compressor specific boundary conditions. Furthermore, we showed that common erosion rate models are not applicable for the materials, test rig setup, and the boundary conditions used in this work.

NOMENCLATURE

A	area
CK	parameter Grant erosion model
D	piping diameters test rig
d_P	particle size
E	erosion rate
$\widetilde{E}$	volumetric erosion rate
$\overline{E}$	empirical mean of erosion rate
$\Delta\overline{E}$	confidence interval of mean erosion rate
GUM	guide to the expression of uncertainty
HV	Vicker's Hardness
ISA	International Standard Atmosphere
$k_{1\ldots3}$	parameters Grant erosion model
$p_{1\ldots5}$	parameters Oka erosion model
Ma	Mach number
MTO	maximum take-off rating
m_M	mass target material removed
m_P	mass impacting particles
N	samples
v_F	fluid velocity
v_p	velocity erosive particles
Re	Reynolds number
s	empirical standard deviation
T_0	absolute temperature
t	t-value of Student t-distribution
x	coordinate along main stream
α	impact angle erosive particle
$\alpha_{E,\max}$	impact angle at max. erosion rate
ϵ	roughness height
κ	isentropic exponent
λ	Darcy friction factor
ρ_M	density target material
σ	standard deviation of the normal distribution
$\widehat{\diamondsuit}$	average of values at pos. x_1 and x_2
$\diamondsuit_{1,2}$	value at position x_1 or x_2

1. INTRODUCTION

We will introduce the topic of blade erosion in axial compressors and its testing in three steps. First, the effect of erosion on compressor blades is presented. Second, the physics behind erosion and two existing erosion rate models are explained. Third, experimental erosion testing and test rigs presented in the literature are reviewed.

1.1. Erosion of axial compressor blades

Erosion of aircraft engines due to ingested, airborne particles mainly affects compressor blades [1, 2], resulting in compressor performance loss and maintenance increase since material from the blades is removed [3]. Erosion is very dependent on compressor type and geometry [4] as well as operational flight environment [5]. Material removal individually changes blade features, resulting in a highly complex and poorly observable system [6].

Side effects of blade material removal are blunted leading edges, reduced chord lengths and blade spans, sharpened trailing edges, and thinning of pres-

sure sides (see Fig. 1) [3]. Blunted leading edges and blade span reduction in particular, are main contributors to compressor performance degradation [7], causing an increase of 3 % or more in specific fuel consumption of the overall engine [8].

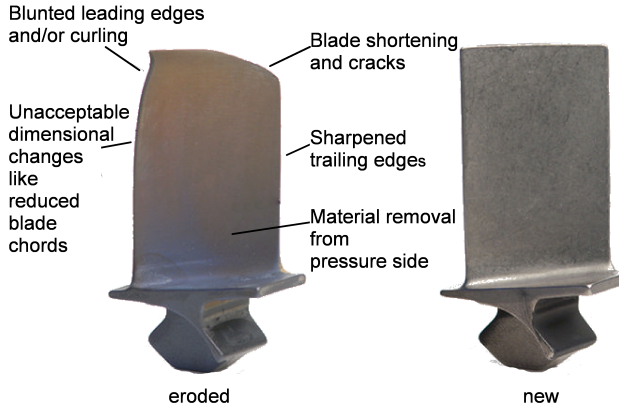

Fig. 1: Comparison of eroded and new compressor blade [3]

Prediction of erosion damage is indispensable for aircraft engine manufactures, operators, and maintenance providers for the following reasons:

- robust design against erosion damage, and
- prediction of maintenance workload and frequency.

1.2. Erosion of engineering metals

In the literature, erosion of engineering metals is generally described as the erosion rate E:

$$(1) \quad E = \frac{m_\mathrm{M}}{m_\mathrm{P}} = f\left(v_\mathrm{P}, \alpha, \dots\right),$$

where m_M is the removed mass of the target material and m_P the mass of impacting erosive particles. The erosion rate is a function of:

- the particle velocity v_P,
- the particle shape and impact angle α, and
- the particle and target material properties, etc.

Erosion of engineering metals is generally divided into brittle and ductile erosion [9]. Since ductile materials are used in compressors of jet engines, only ductile erosion models are considered in this work.

Fig. 2 schematically depicts a single particle impact in a ductile target material. An erosive particle with mass m_P and velocity v_P impacts the target surface at an impact angle α. This primary erosion forms an impact crater and a crater lip. The target material removal by the primary impact and the removal of the crater lip by multiple impacts causes erosion [10, 11]. The maximum erosion rate is observed at impact angles of about $\alpha_{E,\max} = 15° - 30°$ [9,11]. The debris of the target material and the erosive particle cause secondary erosion [12].

Since the 1960s researchers have developed models for predicting the erosion rate [1]. We have selected

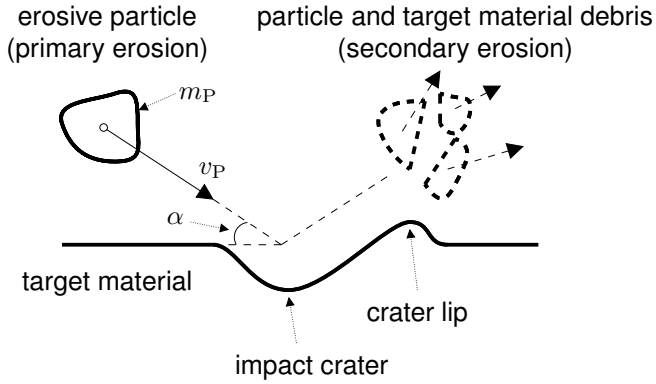

Fig. 2: Schematic drawing of single particle impact in ductile target material [10, 13–15]

two erosion models. The erosion model of Grant and Tabakoff, which is used by many authors, is defined as follows [16, 17]:

$$(2) \quad E = k_1 f_1\left(\alpha\right) v_\mathrm{P}^2 \cos^2\left(\alpha\right)\left[1 - R_\mathrm{T}^2\left(\alpha\right)\right] + f_2\left(\alpha\right)$$

$$(3) \quad f_1\left(\alpha\right) = 1 + CK\left[k_2 \sin\left(\frac{\alpha\pi}{2\alpha_{E,\max}}\right)\right]^2$$

$$(4) \quad f_2\left(\alpha\right) = k_3\left[v_\mathrm{P}\sin\left(\alpha\right)\right]^4$$

$$(5) \quad R_\mathrm{T}\left(\alpha\right) = 1 - 0,0016\, v_\mathrm{P}\sin\left(\alpha\right)$$

$$(6) \quad CK = \begin{cases} 1 & \alpha_\mathrm{P} \le 2\alpha_{E,\max} \\ 0 & \alpha_\mathrm{P} > 2\alpha_{E,\max} \end{cases}$$

where $k_{1\dots3}$ are material parameters. The function $R_\mathrm{T}\left(\alpha\right)$ takes the differences between the tangential component of the impacting and rebounding particle velocity into account and was empirically determined. The model was developed using erosion measurements of 2024 aluminum alloy at particle speeds of $v_\mathrm{P} = 61\,\mathrm{m\,s^{-1}} - 183\,\mathrm{m\,s^{-1}}$. Quartz sand and aluminum particles were used as erodents [16, 17].

A second model was developed by Oka et al. [18, 19], here the erosion rate is defined as target material volume loss per mass of impacting particles ($[\widetilde{E}] = \mathrm{mm^3\,g^{-1}}$):

$$(7) \quad \widetilde{E}\left(\alpha\right) = g\left(\alpha\right)\widetilde{E}_{90}$$

$$(8) \quad \widetilde{E}_{90}\left(\alpha\right) = p_5\, HV^{p_4} v_\mathrm{P}^{p_1}$$

$$(9) \quad g\left(\alpha\right) = \sin^{p_2}\left(\alpha\right)\left[1 + HV\left(1 - \sin\left(\alpha\right)\right)\right]^{p_3}$$

where HV is the Vicker's Hardness of the target material and $p_{1\dots5}$ are material parameters.

The model was developed using single particle impacts on a variety of engineering metals. Three dif-

ferent particle materials were used. The particle impact velocities were $v_\mathrm{P} = 50\,\mathrm{m\,s^{-1}} - 167\,\mathrm{m\,s^{-1}}$.

For the comparison of the Grant and Oka erosion models, the erosion rate E can be calculated from the volumetric erosion rate $\widetilde{E}$ with the target material density ρ_M:

$$E = \rho_\mathrm{M} \cdot \widetilde{E}. \quad (10)$$

So far, no model was developed that uses only available physical or mechanical material parameters, such as density, hardness, yield strength, fracture toughness, etc. [20]. Furthermore, each model uses its own erosion specific material parameters that have to be determined experimentally and cannot be transformed into each other [20]. These parameters are strongly dependent on particle velocities, particle and target material combination, and geometry [21]. Thus, experimental work under high-pressure compressor specific boundary conditions is indispensable for the investigation of erosion in jet engines.

1.3. Erosion test rigs

Since the 1970s experimental erosion tests have been documented in the literature. The research carried out ranges from single blade or cascade up to full-scale gas turbine erosion test set-ups. Hamed et al. [1] provide an overview of erosion tests with their specific testing conditions.

Fundamental effects of erosion are commonly tested in small-scale rigs with single specimens (e.g. flat plates). The particles are typically accelerated centrifugally with a rotating disk (centrifugal test rig) or by a constant fluid stream (gas blast test rig) [20]. For the investigation of compressor blade erosion, the centrifugal test rig is disadvantageous since a containment for the rotating disk is needed that prevents optical accessibility. Moreover, particles that have impacted the target material once need to be hindered from impacting the target again to prevent secondary erosion. Hence, a gas blast type test rig was used for the erosion experiments in this work.

Most of the erosion tests for materials used in jet engines that are described in the literature have particle velocities lower than $v_\mathrm{P} = 200\,\mathrm{m\,s^{-1}}$. Since relative fluid velocities in the first stages of high-pressure compressors are higher and erosion damage is strongly dependent on the velocity we have designed a test rig that provides fluid velocities higher than $300\,\mathrm{m\,s^{-1}}$.

In the following, we will present our work in four parts. First, the development and commissioning process of the high-speed erosion test rig is presented. Second, we show the measurement procedure to determine the erosion rate out of flat plate experiments. Third, the results are shown and discussed. Fourth, conclusions are drawn and an outlook for future work is given.

2. TEST RIG

2.1. Design considerations and boundary conditions

The design considerations and assumptions for the test rig are the following:

- Main effects of compressor erosion phenomena can be investigated with a gas-blast type test rig.
- Particle velocities in in-service high-pressure compressors are not known in contrast to fluid velocities. Thus, when the particle acceleration section in the test rig has a similar length as a compressor stage, particle velocities are assumed to be similar to reality when fluid velocities are the same.
- Runway and near ground particle mass distributions and concentrations do not necessarily correlate with those found in in-service compressors since fan nose cone, centrifugal forces, and secondary erosion influence them. Therefore, standardized test dust, Arizona-Dust A3 with particle sizes of $d_\mathrm{P} = 1\,\mu\mathrm{m} - 120\,\mu\mathrm{m}$ [22], was used as erosive particles in this work.
- Erosion of compressor blades correlates with total particle impacts [2]. Thus, in-service erosion can be accelerated by a higher particle concentration in the test rig than in reality.
- Since erosion damage of jet engines is dominated by the number of take-offs [5], worst case take-off conditions are used as boundary conditions (see Tab. 1) for the test rig design.
- Erosion of compressor blades occurs mainly at the outer 50 % of the blade span [1] (see Fig. 1). Thus, performance calculations for the determination of the fluid parameters will be performed in the middle of the erosive area at 75 % blade span.
- Hot-rolled plates out of Ti6Al4V show fundamentally the same erosion effects as isothermal forged compressor blades out of the same material.

Based on the boundary conditions given in Tab. 1, the relevant performance parameters for a representative high-pressure compressor at the inlet of the 3rd stage at 75 % blade span were calculated for worst case conditions (MTO, ISA +20 K) [23]. The parameters relative to the blade are given in Tab. 2.

Tab. 1: Boundary conditions for performance calculations

Parameter	Value	Unit
rating	MTO	–
ambient temperature	308.15	K
ambient pressure	1013.25	hPa
flight Mach number	0	–

2.2. Test rig design

A schematic drawing of the erosion test rig is depicted in Fig. 3. Air is supplied by a compressor and

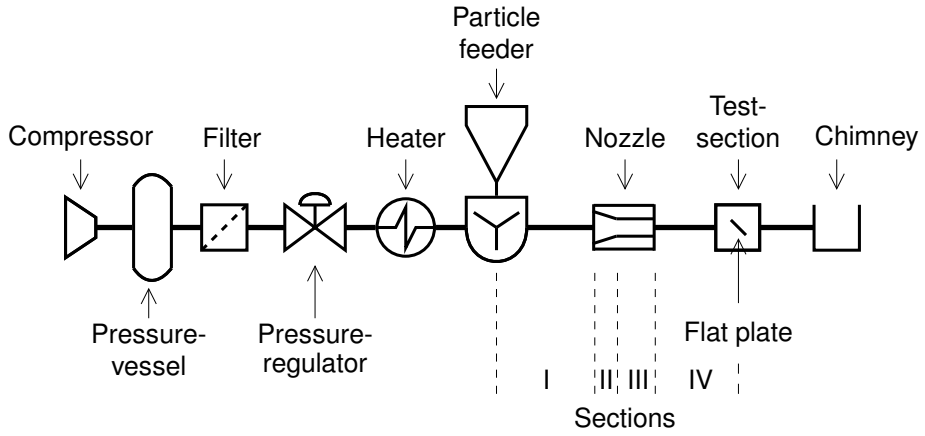

Fig. 3: Schematic drawing of main components of erosion test rig. Section I: mixing tube, II: convergent part of nozzle, III: acceleration part of nozzle, IV: free stream

Tab. 2: Performance calculations of representative high-pressure compressor at 3rd stage inlet at 75 % blade span, all parameters are relative to the blade [23]

Parameter	Value	Unit
relative fluid velocity	350	ms^{-1}
relative Mach number	0.8	–
static temperature	525	K

buffered in a pressure vessel, which damps pressure fluctuations. A micro-filter provides particle-, moisture-, and oil-free air for the erosion tests. The velocity and temperature of the erosive free jet exiting the convergent nozzle are controlled by a pressure regulator and an air heater. The erosive particles are dispersed and injected in the test rig by a particle feeder, which is installed downstream the heater. The particle feeder is removable in order to weigh the mass of the dispersed particles.

The particles run through for four sections (see Fig. 3):

I particle ingestion and dispersion

II acceleration of fluid to maximum velocity and pre-acceleration of particles in convergent part of nozzle

III acceleration of particles in part of nozzle with constant diameter

IV further acceleration of particles in core of free stream and impact on flat plate inside test section.

2.3. Design calculations

The design calculations were performed in two steps. First, the geometries of the test rig (piping length, diameters, etc.) were determined to satisfy the boundary conditions given in Tab. 2 and the performance characteristics of the test rig compressor. These calculations were made without considering the particles. Second, the results were coupled with particle path simulations to approximate the particle velocities in the test section. This approach is valid since the particle concentrations used in the erosions tests are so low that particle-particle and particle-fluid interactions are negligible [23].

2.3.1. Calculations without particles

The working equation based on the stream filament theory for a one-dimensional compressible flow for the current problem is given by Shapiro [24]:

$$\mathrm{d}Ma^2 = F_\mathrm{A}\frac{\mathrm{d}A}{A} + F_{T_0}\frac{\mathrm{d}T_0}{T_0} + F_\mathrm{f}\lambda\frac{\mathrm{d}x}{D}. \tag{11}$$

This equation can be rewritten in the form of finite differences:

$$Ma_2^2 - Ma_1^2 = \widehat{F}_\mathrm{A}\frac{A_2 - A_1}{\widehat{A}} + \widehat{F}_{T_0}\frac{T_{0,2} - T_{0,1}}{\widehat{T_0}} + \widehat{F}_\mathrm{f}\lambda\frac{x_2 - x_1}{\widehat{D}}, \tag{12}$$

$$\widehat{F}_\mathrm{A} = -\frac{2\widehat{Ma}^2\left(1 + \frac{\kappa-1}{2}\widehat{Ma}^2\right)}{1 - \widehat{Ma}^2}, \tag{13}$$

$$\widehat{F}_{T_0} = \frac{\widehat{Ma}^2\left(1 + \kappa\widehat{Ma}^2\right)\left(1 + \frac{\kappa-1}{2}\widehat{Ma}^2\right)}{1 - \widehat{Ma}^2}, \tag{14}$$

$$\widehat{F}_\mathrm{f} = \frac{\kappa\widehat{Ma}^4\left(1 + \frac{\kappa-1}{2}\widehat{Ma}^2\right)}{1 - \widehat{Ma}^2}, \tag{15}$$

where λ is the Darcy friction factor, which is iteratively calculated with the Colebrook-Equation [25]:

$$\frac{1}{\sqrt{\lambda}} = -2\log_{10}\left(\frac{2.51}{Re\sqrt{\lambda}} + 0.27\frac{\epsilon}{D}\right), \tag{16}$$

where ϵ is the roughness height. Eq. 16 is valid in the following range [25]:

$$25 < \frac{\epsilon}{D} Re^{0.875} < 350, \quad (17)$$

this requirement was checked and fulfilled in all calculations.

The geometry was discretized into finite sections Δx along the main stream coordinate x and at each section Eq. 12 was solved iteratively using the boundary conditions listed in Tab. 1. The results in terms of theoretical adjustment ranges of the significant flow parameters at the flat plate in the test section are listed in Tab. 3.

Tab. 3: Calculated performance data of erosion test rig at the flat plate (end of section IV) [23]

Parameter	Value	Unit
fluid velocity	20 – 400	$\mathrm{m\,s^{-1}}$
relative Mach number	0.1 – 1	–
mass flow	0 – 35	$\mathrm{g\,s^{-1}}$
static temperature	253 – 600	K
particle concentration	100 – 500	$\mathrm{mg\,m^{-3}}$

2.3.2. Calculation of particle velocites

The differential equation that governs the movement of a spherical particle on a one-dimensional stream line neglecting gravity, wall friction, particle-particle, and particle-fluid interactions is the following [23]:

$$x'' = \frac{3 c_\mathrm{D} \rho_\mathrm{F}}{4 d_\mathrm{P} \rho_\mathrm{P}} (x')^2 , \quad (18)$$

where ρ_F and ρ_P are the densities of both the fluid and the particles and c_D is the drag coefficient of the particles that is given by Haider und Levenspiel [26] for the Reynolds numbers occurring in the test rig ($Re < 2.6 \times 10^5$):

$$c_\mathrm{D} = \frac{24}{Re} \left(1 + 0.1806 Re^{0.6459}\right) + \frac{0.4251}{1 + \frac{6880.95}{Re}}. \quad (19)$$

Eq. 18 was solved numerically using the boundary conditions given by the calculations performed in the previous section. The results of both calculations are depicted in Fig. 4. The acceleration of the fluid and the particles with different sizes through sections I-IV in the test rig is shown. The abscissa shows the relative length from particle insertion to the position of the flat plate in the test section. The results in Fig. 4 represent a lower bound for the particle velocities since the particles used in the erosion tests have a larger drag coefficient than spheres [27].

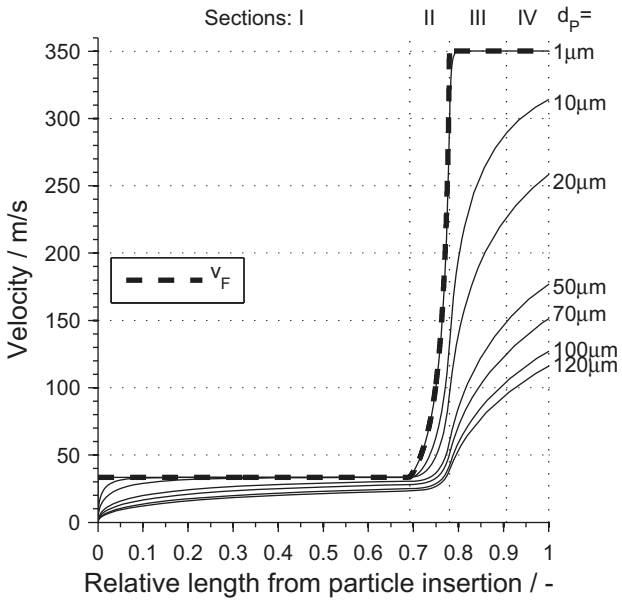

Fig. 4: Fluid v_F and particle v_P velocities for different particle sizes d_P. Sections correspond to those in Fig. 3.

2.4. Commissioning

Based on the geometries and diameters calculated in the section above, the test rig was built. The calculated performance data from Tab. 2 were verified with pressure and temperature measurements in the test section. Therefore, a Pitot tube and a thermocouple were mounted in the test section at the nozzle exit and the test rig was run without ingested particles to prevent damage of the probes. Furthermore, the measurement system was calibrated and the controller parameters were set.

The adjustment accuracy of the fluid velocity, temperature, and Mach number due to pressure fluctuations of the compressor and measurement uncertainty of the measurement system were determined. Therefore, methods provided by the "guide to the expression of uncertainty in measurement" (GUM) were used [28, 29]. Tab. 4 lists the calculated values for a standard error within a 95.4 % (2σ) confidence limit.

Tab. 4: Adjustment uncertainties of erosion test rig calculated with the GUM

Parameter	Value	Unit
relative fluid velocity	$\pm$3.98	$\mathrm{m\,s^{-1}}$
relative Mach number	$\pm$0.01	–
temperature at nozzle exit	$\pm$9.85	K

The effect of the test rig and the mounting and handling of the flat plates on the erosion measurements were also investigated. Therefore, the rig was run without dispersed particles. Results showed that the mass change of the flat plate was insignificant. Thus,

the erosion rate measurement is only dependent on the inserted particles.

3. MEASUREMENT PROCEDURE

This section describes the measurement procedure to acquire the empirical erosion rate E, according to Eq. 1, based on erosion tests of flat plates in three steps. First, the weighting of the flat plates and the particles is described, second the operation of the erosion test rig is presented, and finally statistical methods to gain the experimental erosion test rate are shown.

The mass of the removed target material m_{M} was determined by weighing the flat plates before and after the erosion tests with an analytical balance (readability $0.1\,\mathrm{mg}$). Before each measurement, the plates were ultrasonically cleaned. Furthermore, reference weights were used at each measurement to compensate for altering environmental conditions (e.g. temperature and humidity).

The mass of the impacting particles m_{P} was measured by weighing the whole particle feeder (see Fig. 3) before and after each erosion test. Therefore, the non-negligible amount of particles that was left in the feeder due to electrostatic charge was not accounted for in the erosion rate calculations.

Before each erosion test a flat plate was mounted in the test section and the impact angle α was set by rotating the plate correspondingly. Then, the actual testing was carried out in three steps:

1. heat up (15 min),
2. ingestion of particles until particle dispenser was empty (150 min), and
3. cool down (15 min).

This procedure ensured a thorough heating of the test rig structure and therefore stable operating conditions and low temperatures after the erosion test to demount the flat plates safely.

Two parameters were varied in the erosion tests for this work: the impact angle α and the fluid velocity v_{F}. Since only a limited number ($N = 2 \ldots 5$) of tests was performed for each parameter set (α, v_{F}) the Student-t distribution was used to estimate the confidence interval of the mean erosion rate for each parameter set.

The experimental mean value of the erosion rate is given by:

$$\overline{E}\left(\alpha, v_{\mathrm{F}}\right) = \frac{1}{N}\sum_{i=1}^{N} E_i\left(\alpha, v_{\mathrm{F}}\right), \tag{20}$$

where $E_i\left(\alpha, v_{\mathrm{F}}\right)$ is the erosion rate of an individual test. Furthermore, the empirical standard deviation of the erosion rate is defined by:

$$s\left(\alpha, v_{\mathrm{F}}\right) = \sqrt{\frac{1}{N-1}\sum_{i=1}^{N}\left(E_i\left(\alpha, v_{\mathrm{F}}\right) - \overline{E}\left(\alpha, v_{\mathrm{F}}\right)\right)^2}. \tag{21}$$

Using Eqn. 20 and 21, the experimental erosion rate within a certain confidence interval can be determined:

$$E\left(\alpha, v_{\mathrm{F}}\right) = \overline{E}\left(\alpha, v_{\mathrm{F}}\right) \pm \frac{t \cdot s\left(\alpha, v_{\mathrm{F}}\right)}{\sqrt{N}}, \tag{22}$$

where t is the t-value of the Student t-distribution, which is a function of the confidence level and the number of samples N. For all calculations in this work we chose a two-sided confident level of $95.4\,\%$ (2σ).

The interval of Eq. 22 includes all stochastic errors during the erosion tests and the weight measurements (mounting errors, test rig deterioration, humidity and temperature changes, particle batch, specimen handling, etc.). To fully account for these errors, the parameter set at each erosion test was randomly selected. This means that for a given parameter set the N erosion tests were performed randomly by different people on different days with renewed settings of the impact angle α.

4. RESULTS AND DISCUSSION

Overall, 55 flat plates out of Ti6Al4V were eroded in the test rig. The dimensions of the plates were $50\,\mathrm{mm} \times 50\,\mathrm{mm} \times 4\,\mathrm{mm}$ and the Vickers hardness of the material was $(376 \pm 3)\,HV\ 5$. The plates were eroded with fluid velocities of $v_{\mathrm{F}} = 300\,\mathrm{m\,s^{-1}}$ and $v_{\mathrm{F}} = 350\,\mathrm{m\,s^{-1}}$ at eleven impact angles and $m_{\mathrm{P}} = 55\,\mathrm{g}$ Arizona Dust A3 was used as erosive particles. The particles were uniformly dispensed in $150\,\mathrm{min}$, yielding to a mean particle concentration of approximately $222\,\mathrm{mg\,m^{-3}}$.

Fig. 5 shows the erosion curves. For every data point shown at least $N = 2$ erosion tests were performed. At $300\,\mathrm{m\,s^{-1}}$ the maximum erosion rate was $E_{\max} = 1.289\,\mathrm{mg\,g^{-1}}$ at an angle of $16°$. At $350\,\mathrm{m\,s^{-1}}$ the maximum erosion rate was $E_{\max} = 1.804\,\mathrm{mg\,g^{-1}}$ at an angle of $16.3°$.

The error bars were calculated using Eq. 22. The different sizes of the erosion bars show how stochastic errors can affect the testing and measurement process.

The erosion curves for angles lower than $60°$ showed typical patterns for ductile metals, with a peaking erosion rate between $15° - 30°$ followed by a strictly monotonic decrease. However, between $\alpha = 60° - 80°$ a plateau of nearly constant erosion rates occurred before the erosion rates decreased again.

The parameters for the Grant (Eqn. 2-5) and Oka (Eqn. 7-9) erosion models were calculated with a nonlinear least-squares regression. Since the combined

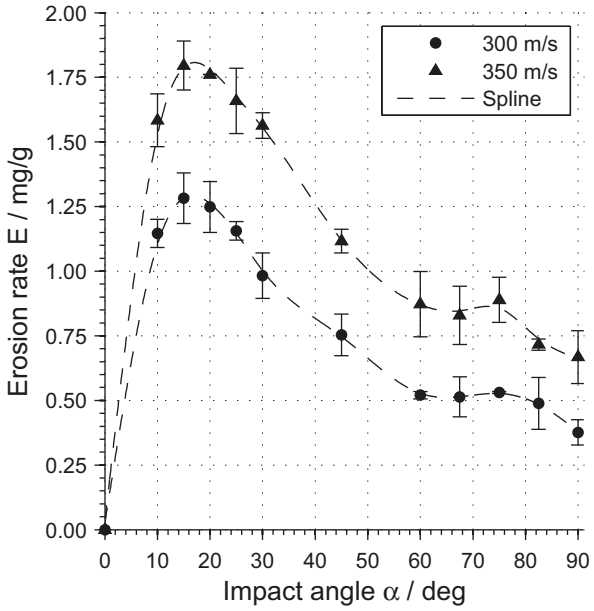

Fig. 5: Erosion curves of flat plates out of Ti6Al4V

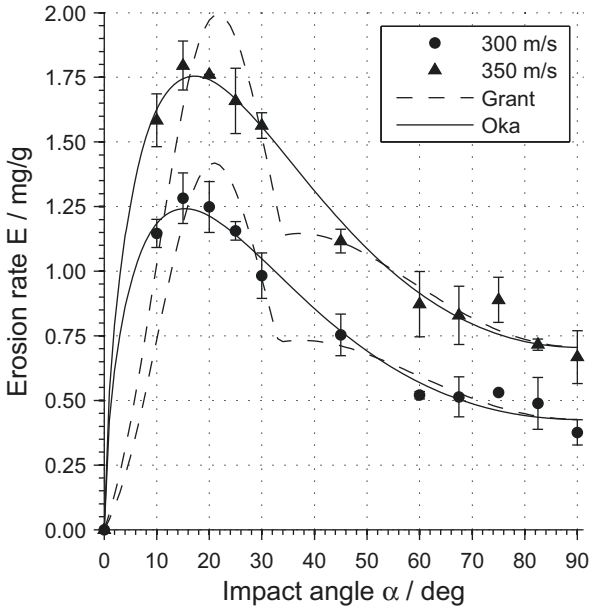

Fig. 6: Application of erosion models of Grant and Oka for the measured erosion rates.

Tab. 5: Parameters of Grant (Eq. 2) and Oka (Eq. 7) erosion models, for the curves depicted in Fig. 6

		v_F	
		$300\,\mathrm{m\,s^{-1}}$	$350\,\mathrm{m\,s^{-1}}$
Grant Eq. 2	k_1	2.8578×10^{-5}	2.5381×10^{-5}
	k_2	0.5529	0.4727
	k_3	4.2578×10^{-11}	4.0286×10^{-11}
Oka Eq. 7	p_1	1.8956	1.9089
	p_2	0.6006	0.6194
	p_3	7.5975	7.0911
	p_4	2.6085	2.5458
	p_5	4.0823×10^{-2}	4.3885×10^{-2}

fitting for both fluid velocities resulted in non-satisfying results, a parameter set was calculated for each velocity and model. Moreover, both models use the particle velocity to determine the erosion rate. Since the particle velocities were not measured and were not equal due to different particle sizes (see Fig. 4) we used the fluid velocity instead. The results are depicted in Fig. 6 and the parameters for both models are listed in Tab. 5.

The erosion rate model of Grant and Tabakoff (Eq. 2) diverges significantly from the measured data points. Moreover, the function $f_2\,(\alpha)$ vanishes, since the constant k_3 is orders of magnitude lower than the erosion rate. The Oka model showed good correspondence with the measured data at impact angles of $\alpha = 0° - 60°$. The plateau between $\alpha = 60° - 80°$ is not resolved by both models, respectively.

Therefore, we conclude that both models are not generally applicable for the target and material combination, fluid and particle velocities, and test rig set-up as used in this work. Especially the velocity distribution of the particles, caused by the dimensions of the nozzle and the particle sizes, seemed to influence the erosion characteristics significantly. This finding supports the assumption of [20] that erosion needs to be investigated experimentally until an applicable model is available.

5. CONCLUSIONS AND FUTURE WORK

A high-speed erosion test rig was designed, built, and commissioned, which is capable of providing boundary conditions for the investigation of the main effect of axial compressor blade erosion. Flat plates out of Ti6Al4V were eroded with altering impact angles and fluid velocities. The following conclusions were made:

- The erosion test rig presented in this work was capable of measuring erosion rate curves reproducibly.
- The erosion models of Oka and Grant cannot be extrapolated to the velocities, materials and test rig setup used in this work.
- Flat plates out of Ti6Al4V showed erosion patterns typical for ductile metals at impact angles of $\alpha = 0° - 60°$.
- The erosion curve of Ti6Al4V showed a plateau between the impact angles $\alpha = 60° - 80°$.

In future works we will use laser shadowgraphy and Interferometric Mie Imaging to directly measure the particle velocities in the test section. Furthermore, we will use different test specimens (e.g. cylinders, blades) out of aluminum to investigate the geometric change of shape caused by erosive particles.

REFERENCES

[1] Hamed, A., Tabakoff, W., and Wenglarz, R., 2006. "Erosion and Deposition in Turbomachinery". *Journal of Propulsion and Power, 22*(2), pp. 350–360.

[2] Grieb, H., 2009. *Verdichter für Turbo-Flugtriebwerke*. Springer-Verlag Berlin Heidelberg.

[3] Heutling, F., Uihlein, T., Brendel, T., Eichmann, W., and Ücker, M., 2010. Erosionsschutz für Titan- und Superlegierungen. Tech. rep., MTU Aero Engines GmbH.

[4] Edwards, V., and Rouse, P., 1994. "U.S. Army Rotorcraft Turboshaft Engines - Sand & Dust Erosion Consinderations". *AGARD Conference Proceedings, 558*, pp. 3.1–3.10.

[5] Schirmeister, F., 2013. "Untersuchungen zum Einfluss der Betriebsbedingungen auf die Leistungsverschlechterung von Turboluftstrahltriebwerken". PhD thesis, Universität Stuttgart.

[6] Schrade, M., Staudacher, S., Weissschuh, M., and Voigt, M., 2012. "Form Factor for the Top-Level Comparison of the Condition of Supply of High-Pressure Compressor Blades". In ASME 2012 Gas Turbine India Conference, GTIndia 2012-9599.

[7] Ghenaiet, A., Tan, S., and Elder, R., 2005. "Prediction of an axial turbomachine performance degradation due to sand ingestion". *Proceedings of the Institution of Mechanical Engineers, Part A: Journal of Power and Energy, 219*(4), Jan., pp. 273–287.

[8] Kumar, A., Nair, P., Keane, A., and Shahpar, S., 2005. "Probabilistic Performance Analysis of Eroded Compressor Fan Blades". *ASME Power PWR2005-50070*.

[9] Aquaro, D., and Fontani, E., 2002. "Erosion of Ductile and Brittle Materials". *Meccanica, 36*(6), pp. 651–661.

[10] Rossmann, A., 2006. *Die Sicherheit von Turbo-Flugtriebwerken. 1. Einführung, Schadensanalyse, Fremdkörper, Umgebungseinflüsse*. Turbo Consult, Rossmann.

[11] Kosel, T. H., 1992. "Solid Particle Erosion". In *ASM Handbook, Volume 18: Friction, Lubrication, and Wear Technology*, Vol. 18. pp. 199–213.

[12] Tilly, G., 1973. "A two stage mechanism of ductile erosion". *Wear, 23*(1), Jan., pp. 87–96.

[13] Hutchings, I., and Winter, R., 1974. "Particle erosion of ductile metals: A mechanism of material removal". *Wear, 27*(1), Jan., pp. 121–128.

[14] Oka, Y., and Nagahashi, K., 2003. "Measurements of plastic strain around indentations caused by the impact of round and angular particles, and the origin of erosion". *Wear, 254*(12), Nov., pp. 1267–1275.

[15] Cenna, A., Page, N., Kisi, E., and Jones, M., 2011. "Single particle impact tests using gas gun and analysis of high strain-rate impact events in ductile materials". *Wear, 271*(9-10), July, pp. 1497–1503.

[16] Grant, G., Tabakoff, W., and Ball, R., 1974. "An Experimental Investigation of certain Aerodynamic Effects on Erosion". *AAIA Paper No. 74-639*.

[17] Grant, G., and Tabakoff, W., 1975. "Erosion Prediction in Turbomachinery Resulting from Environmental Solid Particles". *Journal of Aircraft, 12*(5), pp. 471–478.

[18] Oka, Y., Olmogi, H., Hosokawa, T., and Matsumura, M., 1997. "The impact angle dependence of erosion damage caused by solid particle impact".

[19] Oka, Y., and Yoshida, T., 2005. "Practical estimation of erosion damage caused by solid particle impact". *Wear, 259*(1-6), July, pp. 102–109.

[20] Meng, H., and Ludema, K., 1995. "Wear models and predictive equations: their form and content". *Wear, 181-183*, pp. 443–457.

[21] Sommer, K., Heinz, R., and Schöfer, J., 2010. *Verschleiss metallischer Werkstoffe*. Vieweg+Teubner, Wiesbaden.

[22] ISO 12103-1:1997-12. Road vehicles - Test dust for filter evaluation - Part 1: Arizona test dust.

[23] Illg, J., 2012. "Vorauslegung eines Versuchsstands zur Ermittlung von Erosionsschädigungen von Verdichterschaufeln". Diplomarbeit, Institut für Luftfahrtantriebe, Universität Stuttgart.

[24] Shapiro, A. H., 1953. *The Dynamics and Thermodynamics of Compressible Fluid Flow, Vol. 1*. The Ronald Press Company, New York.

[25] Sigloch, H., 2011. *Technische Fluidmechanik*. Springer, Dordrecht Heidelberg London New York.

[26] Haider, A., and Levenspiel, O., 1989. "Drag Coefficient and Terminal Velocity of Spherical and Nonspherical Particles". *Powder Technology, 58*, pp. 63–70.

[27] Fletscher, R., and Bright, D., 2000. "Shape Factors of ISO 12103-A3 (Medium Test Dust)". *Filtration + Separation*(9), pp. 48–52,54–56.

[28] JCGM100:2008, 2008. Evaluation of measurement data - Guide to the expression of uncertainty in measurement.

[29] Chatzianagnostou, D., 2013. "Inbetriebnahme und Kalibrierung eines Versuchsstands zur Ermittlung von Erosionsschädigung von Verdichterschaufeln". Studienarbeit, Institut für Luftfahrtantriebe, Universität Stuttgart.